ROBERT C. BEAL

SPECTRASAT: A HYBRID ROWS/SAR APPROACH TO MONITOR OCEAN WAVES FROM SPACE

Evidence from both Seasat and the Shuttle Imaging Radar indicates that Doppler contamination in synthetic aperture radar (SAR) at the shorter azimuth (along-track) ocean wavelengths can seriously limit the instrument performance. Although the problem is alleviated at low orbital altitudes, it is never completely eliminated, particularly for higher wave slopes. By combining a SAR with a conically scanning altimeter (a radar ocean-wave spectrometer) on a common low-altitude platform, the disadvantages of each tend to be offset by the advantages of the other. Thus, a hybrid combination of the two may be the most practical approach to monitoring ocean waves from space.

INTRODUCTION

Global directional wave estimates will be essential in the future to properly initialize, update, and validate wind-driven wave prediction models. Many of these models use physics that have yet to be verified for any but the simplest wind fields. For example, the growth and evolution of waves in a turning or adverse wind field is a continuing subject of debate. An understanding of the associated physics is essential to improve the accuracy of operational forecasting, particularly as it relates to the life cycle and morphology of ocean storms, within which occur much of the significant energy transfer between the atmosphere and the ocean.

Although many potential techniques exist for monitoring the local directional wave spectrum,[1] only a few are suitable for collecting spectra over global scales, and only the synthetic aperture radar (SAR) has so far been evaluated from orbit.[2,3] However, both the SAR and the radar ocean-wave spectrometer[4] (ROWS) appear to have the potential for spacecraft application and could even complement each other in certain configurations, one of which is outlined in this and further articles in this issue (see Jackson; MacArthur; Kilgus and Frain). There are no plans at present to orbit a ROWS; SARs suitable for observing the ocean have flown on Seasat in 1978 and the Shuttle Imaging Radar Experiment B (SIR-B) in 1984 and are planned for both the European Remote Sensing Satellite (ERS-1) and NASA's SIR-C in the early 1990s.

Robert C. Beal is a principal staff physicist and assistant supervisor of the Space Geophysics Group, The Johns Hopkins University Applied Physics Laboratory, Laurel, MD 20707.

PREVIOUS SEASAT AND SIR-B RESULTS

A Simple Model for Azimuth Motion Blur

SAR ocean-wave spectra are much less contaminated with azimuth motion blur (or filtering) when the platform is both low and fast flying. The relevant platform parameter for comparison is R/V, the ratio of the platform range to its velocity. Harger[5] gives the azimuth displacement, Δx_a, resulting from a moving scatterer with radial velocity v_r as

$$\Delta x_a = \frac{R}{V} v_r . \qquad (1)$$

The radial velocity v_r can be associated with the radial component of the orbital velocity of an ocean wave (where the "orbit" is that of a free surface particle whose radius is approximately the dominant wave height and whose period is the dominant wave period). In reality, the water surface is better described by a complete spectrum of waves. The spectrum has historically been described as fully developed when it approaches an asymptotic spectral form at very large fetch and duration of a uniform wind field. Although the ocean is no longer thought to be so simple (see, for example, Kitaigorodskii, this issue), the concept of full development still has utility for simple models. For a fully developed Pierson-Moskowitz spectrum, the root-mean-square (rms) velocity, v_{rms}, is simply related to the significant wave height (SWH; also denoted by H_s) by

$$v_{\text{rms}} = \left(\frac{\alpha\pi g^2}{4}\right)^{1/4} H_s^{1/2} , \qquad (2)$$

where α is the Phillips constant and g is the gravitational constant. Expressing the result in the Fourier domain and using Eq. 1 combined with a Gaussian assumption for scatterer velocities, Monaldo and Lyzenga[6] find a minimum detectable azimuth wavelength, λ_{min} (defined at the 2σ response level, i.e., 14 percent), of

$$\lambda_{\text{min}} = \frac{\pi\sqrt{2}}{2}\left(\frac{\alpha\pi g^2}{4}\right)^{1/4}\left(\frac{R}{V}\right) H_s^{1/2} , \qquad (3)$$

or, with all units given in the meter-kilogram-second system,

$$\lambda_{\text{min}} \cong 2\left(\frac{R}{V}\right) H_s^{1/2} . \qquad (4)$$

Now let us see how well this simple model fits the experimental data from Seasat and SIR-B.

Evidence of Azimuth Smear in Seasat and SIR-B

Equation 4 predicts that the most severe attenuation of azimuth-traveling waves will occur in the highest sea states and for the higher altitude orbits. (V is only weakly dependent on altitude for ranges that are small compared to the radius of the earth.) For example, in a sea state with an SWH of 4 meters for the SIR-B geometry (R/V approximately 30), λ_{min} is approximately 120 meters. However, the same sea state, when imaged with the Seasat geometry (R/V approximately 130) would yield a λ_{min} of about 520 meters, such an extremely severe limit that practically the only waves visible in Seasat imagery of high sea states would be those traveling orthogonal to the azimuth direction (i.e., range traveling).

Figure 1 shows a set of high sea state examples of SAR ocean-wave spectra for both the high-altitude (800-kilometer) Seasat and the low-altitude (235-kilometer) SIR-B. Superimposed on the spectra are the estimated minimum detectable azimuth wavelengths, calculated from Eq. 4. It is easy to see why there are so very few documented cases of azimuth-traveling waves from the Seasat data set. On the other hand, SIR-B appears to retain appreciable azimuth response even in the active region of a hurricane, where the estimated SWH was 8 to 10 meters.

Clearly then, low-altitude orbits greatly reduce azimuth smear. But even the lowest practical altitude produces spectral distortion under some wave conditions, as the SIR-B intercomparisons will demonstrate.

SIR-B Four-Way Spectral Intercomparisons off the Coast of Chile

The Basis of the Estimates. The primary objective of the SIR-B spectral intercomparisons off the west coast of southern Chile (nominally centered around 55 degrees south latitude, 80 degrees west longitude) was to explore the ability of a spaceborne SAR to monitor the directional wave spectrum over a wide range of sea states. The SAR-derived estimates of the wave spectrum can be compared not only with the more direct wave-height maps of the surface contour radar (SCR) (see Walsh et al., this issue) and slope spectra from the ROWS (see Jackson, following article, in this issue), but also with spectral estimates from the U.S. Navy Global Spectral Ocean-Wave Model (GSOWM) (see Zambresky, this issue).

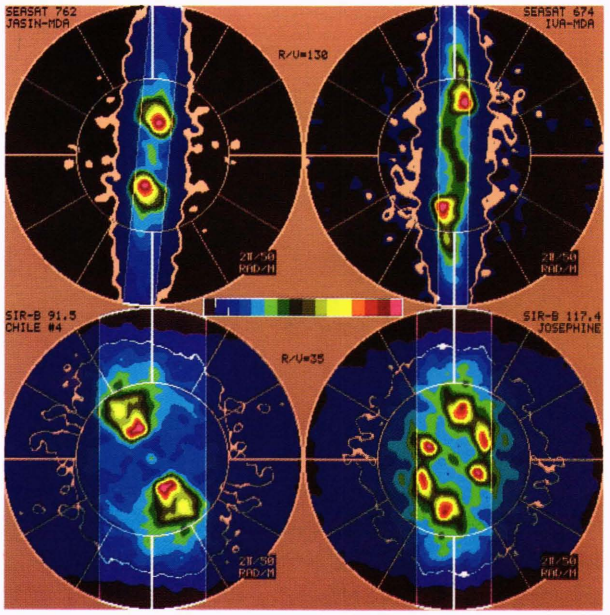

Figure 1—Examples of SAR wavenumber spectra in high sea states for Seasat (top pair: 4.4 meters in the JASIN experiment and 6.4 meters in Hurricane Iva) and SIR-B (bottom pair: 4.4 meters in Chile and 8 to 10 meters in Hurricane Josephine). The azimuth or flight direction is horizontal. The 16-step color scale is linear in image spectral energy density, with each spectrum individually normalized. The lowest (sixteenth) step of the energy densities is coded by a continuous gray scale, and the white contour is chosen at 3σ above the mean noise background. Azimuth wavenumber limits calculated from Eq. 4 are shown shaded. The estimated number of degrees of freedom is at least 1000 for these and all subsequent SAR spectra, resulting in confidence limits well within one color contour.

During the SIR-B experiment, we were fortunate to have collected directional spectra estimates from all four of these sources for four consecutive days (October 9 through October 12, 1984). Also, somewhat fortuitously, the local sea state (as determined by averaging three independent, direct range-measuring instruments on a NASA P-3 aircraft) varied from about 1.7 to about 4.6 meters. All three instrument-based estimates of the spectra (SIR-B, SCR, ROWS) were within 50 kilometers of one another on all days and usually collected within 30 minutes of one another. Data from GSOWM, the fourth of the estimates, were available only discretely every 12 hours in increments of 2.5 degrees latitude by 2.5 degrees longitude; however, they were linearly interpolated in both space and time to agree with the mean of the instrument estimates. Finally, all spectral estimates were

transformed to a common format that displayed spectral energy density (in units of meters to the fourth power) as a function of radian wavenumber. For the SAR, methods described separately by Lyzenga, Monaldo, and Tilley in this issue were applied to yield estimates of the height-variance spectrum. Corrections for azimuth falloff were applied as well. The results of the four daily estimates are shown consecutively by day in the following four figures.

Prior to a detailed comparison, note the following general features of the spectra:

1. All spectra are presented in radian wavenumber coordinates, where the radian wavenumber is equivalent to 2π/wavelength. The outer circle ($2\pi/100$ radians per meter or $2\pi/50$ radians per meter) corresponds to the highest wavenumber, or shortest wavelength, of interest. Only on the third day (the day of lowest sea state) is appreciable energy found at wavelengths shorter than 100 meters.
2. Only the SIR-B spectra are intrinsically radially symmetric, since they are obtained from a "frozen" radar image that is two-fold ambiguous with respect to direction of wave travel. The ROWS spectra can yield slightly different upwind and downwind estimates, but these are minor and have been averaged together here to produce symmetric spectra. The SCR spectra are not symmetric because the "encounter" spectrum of an SCR must be corrected for its finite forward platform velocity; this correction produces asymmetric spectra, only one side of which can generally be identified with the "true" spectrum (see Walsh et al., this issue). The GSOWM spectra are inherently one-sided; in this case, all spectra represent the direction *from which* the waves are approaching. Thus, in Fig. 2, a dominant wave with a length of 200 to 250 meters is approaching *from* the northwest.
3. Each individual spectrum is normalized with a 16-step linear color scale. From aircraft estimates of SWH obtained from the aircraft's three direct range-measuring instruments, each color scale is displayed in absolute energy-density units of meters quadrupled shown in the horizontal scale located under each spectrum. The three directional estimates (SCR, ROWS, SAR) are normalized with the average aircraft estimate of SWH shown in Table 1; the GSOWM spectra are normalized separately with the model estimate of SWH shown in the same table.

Sea State Summary. Table 1 is a summary of all the direct (ranging) aircraft estimates of SWH for each of the four days, showing their daily averages as compared with those from the model. Over the average of the four days, the aircraft estimates and the model are in close agreement. However, the daily variations estimated from the aircraft are much greater than those from the model. The discrepancies are particularly severe for the middle two days, when a local null was followed by a rapid intensification, both of which were apparently entirely missed by the model. This apparent insensitivity to daily variations may be characteristic of GSOWM in the southern hemisphere and can probably be traced to the lack of smaller scale knowledge of the source wind fields, particularly in the southern Pacific. No doubt future global wind measurements from space could do much to correct the problem. In any case, Table 1 shows a broad distribution of wave heights over which we can compare the various estimates of the directional spectra.

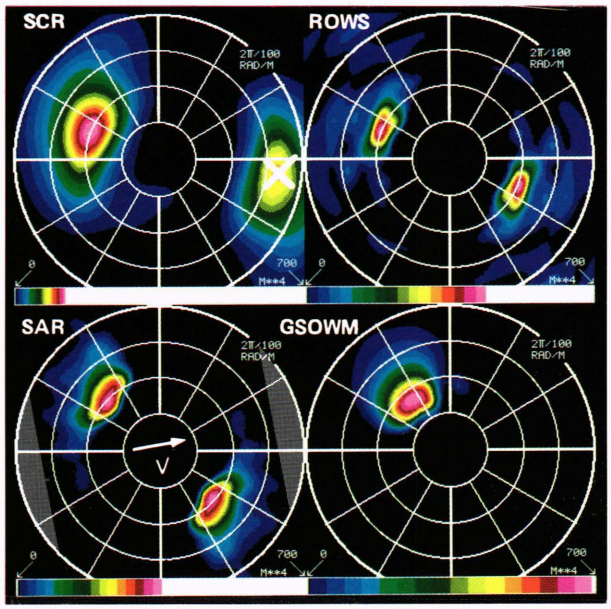

Figure 2—Estimates of wavenumber height-variance spectra for October 9, 1984, color coded in absolute spectral energy density units of meters quadrupled. The outer circle corresponds to a 100-meter wavelength. North is vertical for these and all subsequent spectra. SAR azimuth wavenumber limits calculated from Eq. 4 are shown shaded. The SIR-B velocity vector is shown by the arrow at the center of the SAR spectrum. In Figs. 2, 3, 5, and 6, the false lobes of the SCR are designated by the white crosses.

Table 1—Estimate of significant wave heights (in meters) for the SIR-B Chile experiment.

	Aircraft Instruments				
Date	*SCR*	*Laser Altimeter*	*Radar Altimeter*	*Aircraft Average*	*GSOWM*
Oct 9	2.7	3.2	2.5	2.8	3.5
Oct 10	1.7	–	–	1.7	2.7
Oct 11	4.6	4.4	4.6	4.6	3.0
Oct 12	3.3	3.7	3.5	3.5	3.1
			Average	3.15	3.08

October 9 Spectra ($H_s \approx 2.8$ *m*). Figure 2 shows the set of height-variance spectra for October 9. Both the SCR and the ROWS indicate a single wave system with a 200-meter wavelength approaching the site from about 20 degrees north of west. The major discrepancy between the two estimates appears to lie in the estimated spectral width, with the SCR indicating a considerably broader width than the ROWS, both in angle and wavenumber.

Broadening might be expected from the SCR in its cross-track dimension (which in this case is approximately north–south), since its swath contains only about 50 resolution elements. The SCR broadening in wavenumber (or, alternatively, narrowing by the ROWS) is at present one of the few anomalies in an otherwise consistent set of SCR/ROWS estimates in the four-day series.

Both the SAR and the GSOWM spectra are rotated by nearly 30 degrees with respect to the SCR/ROWS estimates; moreover, the GSOWM-estimated wavelength is greater than the SCR/ROWS/SAR estimates by nearly 20 percent. This is a good example of the SAR experiencing marginally acceptable azimuth contamination. The flight (azimuth) direction is nearly east–west, and the azimuth filter is operating on the high-wavenumber edge of the spectrum to cause an apparent rotation toward the range direction of at least 20 degrees. The similar rotation seen in the GSOWM estimate is only coincidental, as can be verified by noting its similar systematic departure from the SCR/ROWS estimates during the remaining three days of the experiment.

October 10 Spectra ($H_s \approx 1.7$ *m*). Figure 3 shows the set of height-variance spectra for October 10. This data set is unique in several ways. First, the estimated sea state was by far the lowest of all four days. Second, the spectrum (as estimated by the SCR) shows at least three separate wave systems traveling in separate directions and all with different wavelengths. Third, and most important for a test of the SAR performance, the major wave system has a short dominant wavelength (approximately 80 meters), is very broad in angle, and has significant energy at high azimuth (east–west) wavenumbers.

Although even the SCR and ROWS appear to have some difficulty accurately mapping all aspects of this complicated low-energy spectrum, there is at least good agreement on the major features: a primary system about 80 meters long approaching from 30 degrees east of north and a weaker, possibly distinct, secondary system about 100 meters long approaching from either the north or south. (Additional spatially separated spectral estimates could remove this ambiguity.)

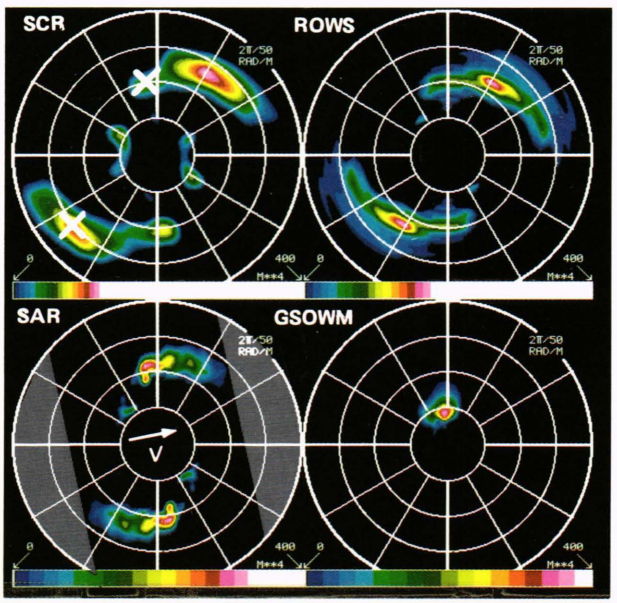

Figure 3—Estimates of wavenumber height-variance spectra for October 10. The outer circle corresponds to a 50-meter wavelength. Calculated SAR azimuth wavenumber limits are shown shaded. The SIR-B velocity vector is shown by the arrow.

This low-energy confused sea state clearly demands too much from the SAR. Severe azimuth filtering acts upon the primary short-wave system essentially to obliterate any signs of its existence. Its filtered remnants appear as a weak secondary system rotated toward range by about 10 degrees. Simultaneously, the secondary (range-traveling) system, having been subjected essentially to no filtering action, now has become the primary system in the SAR's perspective. Without the very detailed picture of this extremely complicated spectrum that is provided by both the SCR and ROWS, the perception could easily be that the SAR has actually "created" a new wave system that previously did not exist. This would be an alarming situation indeed, since it could be interpreted as evidence for a highly nonlinear SAR transfer function acting in an unpredictable (and nonreversible) fashion to map energy from one part of the spectrum to another. In fact, with only a directional buoy to offer "sea truth," such a conclusion might be the only logical one, because in this case even the best buoy analysis would probably identify only a "mean" direction and spectral width and might altogether miss the autonomous nature of the secondary system.

The GSOWM, as the SAR, is severely tested by the very low sea states on this day. GSOWM, in fact, fails to recognize the strong minimum in energy (Table 1) and continues to forecast a single 200-meter-long wave system approaching from the north, only slightly diminished in energy from the previous day. If this 200-meter system is identified with the similar weak long-wave energy seen coming from the west or northwest in the SCR, ROWS, and SAR (long-wave energy cannot have an easterly source in this region of the world), then the GSOWM appears to show a substantial clockwise rotation of its dominant wave system, as it did on the previous day.

October 11 Spectra ($H_s \approx 4.6$ *m*). In the domain of wavenumber *slope*, which is much closer to the actual (uncorrected) output product of both the ROWS and the SAR, the spectra of October 11 (Fig. 4) are bimodal. Furthermore, each wave system approaches the experimental site from an opposing direction. This is shown in Fig. 4 by the opposing spatial evolution of the two systems. The longer wave system rotates counterclockwise and the shorter wave system rotates clockwise as the spectral samples progress toward the east. The remarkable agreement between the two instruments in nearly all aspects of these spatially evolving slope spectra, particularly in a high sea state, is the most compelling evidence from the entire experiment that the SAR possesses the potential, under the right environmental conditions, to make a unique contribution to our understanding of ocean-wave development.

As Fig. 5 shows, the associated height-variance spectra are not bimodal; both the ROWS and SAR spectra

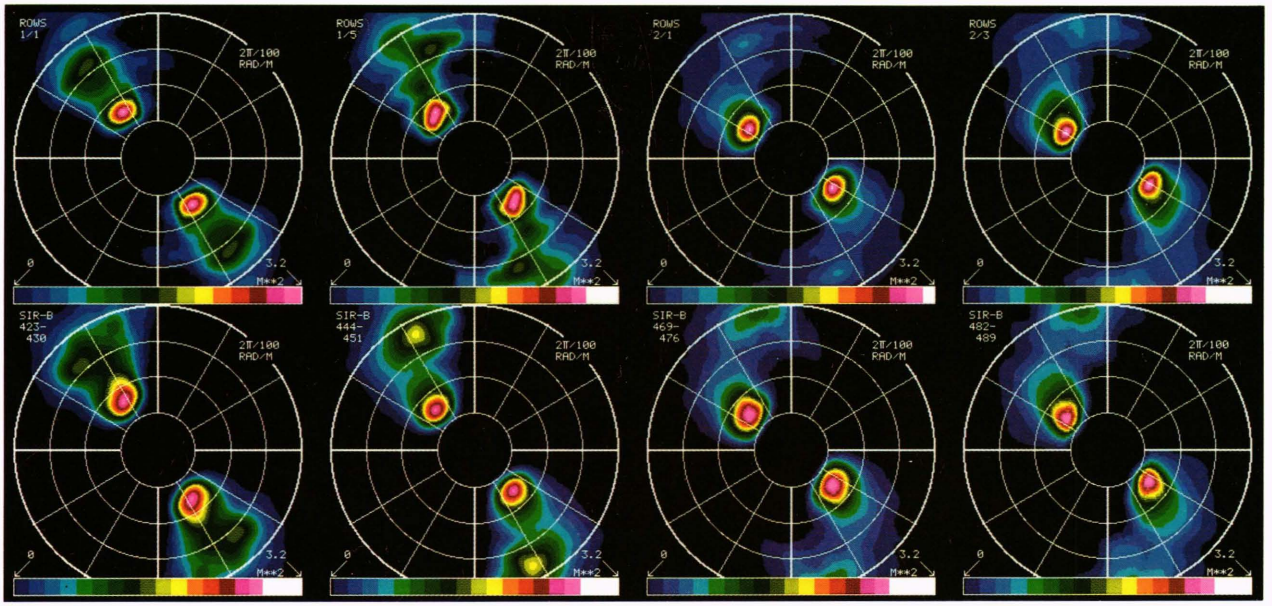

Figure 4—A spatial sequence of four exactly coincident ROWS (top row) and SAR (bottom row) wavenumber slope-variance spectra for October 11. Separation between pairs of adjacent spectra is about 100 kilometers. The left pair is most westerly; the right pair is most easterly. A common absolute scale in meters squared is used for all spectra. The outer circle corresponds to a 100-meter wavelength.

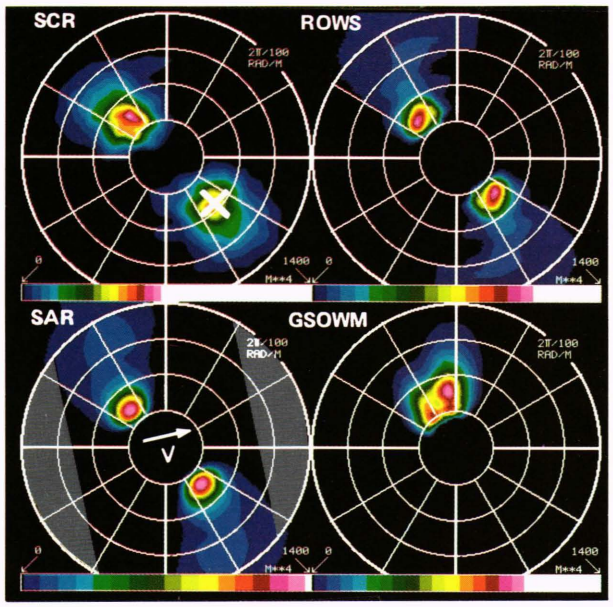

Figure 5—Estimates of wavenumber height-variance spectra for October 11. The outer circle corresponds to a 100-meter wavelength. Calculated SAR azimuth wavenumber limits are shown shaded.

show broad skirts at the higher wavenumbers. Without knowledge of the spatial evolution, this broad skirt might well be misinterpreted as a part of the primary 250-meter-wavelength system approaching from the northwest. With an enlightened perspective made possible with the ROWS and SAR, however, it is clear that the high-wavenumber portion of the spectrum is actually approaching from the southeast, in direct opposition to the primary system.

In this high sea state, the SAR appears to show little sign of azimuth filtering, even for the high-wavenumber system, and shows somewhat better agreement with the ROWS than with the SCR. The circular symmetry of the SAR spectrum around the primary peak is probably the result of relatively greater (and probably unnecessary) spectral smoothing for the SAR. The GSOWM spectrum on this day is unusual, consisting of both a primary and secondary system, both approaching from the northwest quadrant. In contrast to the previous day, GSOWM significantly underestimates the energy here (Table 1) and, for the third day in a row, shows its primary system approaching with a large positive angular discrepancy. This trend will be seen to persist on the succeeding and final day.

October 12 Spectra ($H_s \approx 3.5$ *m*). Figure 6 shows the set of height variance spectra for October 12, the last day of the experiment. Here we have a strong primary system approaching from the west, almost exactly along the azimuth direction of the SAR. The primary wavelength of 400 meters and direction from due west are confirmed in both the SCR and ROWS spectra, with a faint hint of a secondary component traveling nearly orthogonally. This is the longest, but not highest, wave system encountered during the experiment and is probably well removed from its source by this time.

With the excellent confirmation in angle of approach, this data set considerably strengthens the case that the SAR can indeed faithfully reproduce the full spectrum of an azimuth-traveling wave if the energy lies well within the azimuth filter limits. The spectral width in wavenumber appears faithfully reproduced in the SAR spectrum, although some angular broadening may be evident. The GSOWM estimate, while faithfully modeling the long dominant wavelength, continues the unbroken pattern

Figure 6—Estimates of wavenumber height-variance spectra for October 12. The outer circle corresponds to a 100-meter wavelength. Calculated SAR azimuth wavenumber limits are shown shaded.

of indicating a much more northerly approach. This time the angular discrepancy appears to be in excess of 40 degrees.

Comparison of ROWS and SAR Slope-Variance Estimates for All Four Days. In estimating the properties of an ocean wave with amplitude, A, and wavenumber, k, both the ROWS and the SAR tend to yield something closer to slope (Ak) variance spectra than to height (A) variance spectra. Consequently, ROWS/SAR intercomparisons of slope variance can often be more revealing, especially at high wavenumbers.

Figure 7 summarizes the four-day ROWS/SAR slope-variance sequence. The major features of the primary systems shown in the previous figures persist, but the subtleties in the high-wavenumber skirts are more evident here. In the slope domain, multimodal behavior is the rule rather than the exception. Both instruments show multimodal behavior on each of the four days, with lowest correlation on the first two (lower sea-state) days and highest correlation on the last two (higher sea-state) days. As Fig. 4 further confirmed, the remarkable agreement persisted along a several-hundred-kilometer track on the third (highest sea-state) day. These comparisons might be taken as evidence that the subtle variations indicated by the SIR-B spectra in Hurricane Josephine (see Gonzalez et al., this issue) are in fact credible, even in the absence of independent verification.

Summary of All Height-Variance Estimates for All Four Days. A summary of the estimates from all four days can be presented effectively by reproducing only the half-intensity contours of the height-variance spectra from Figs. 2, 3, 5, and 6 and superimposing each of them on a common format for each of the four days. This is done in Fig. 8. Now the similarities and differences in the individual estimates become more obvious. If we define an "acceptable" estimate as one that is correct to within about a half spectral width, then we can reach some judgments as to the acceptability of the various estimates.

The SCR and ROWS "acceptably" agree with each other on all four days, although only marginally on the lowest sea-state day. The SAR is acceptable on the highest sea-state (last two) days, only marginally on the intermediate sea state, and not at all for the very lowest sea state. The GSOWM fails completely to meet the criterion on two days, one of which is the lowest sea state, and meets it only marginally on the other two. Except

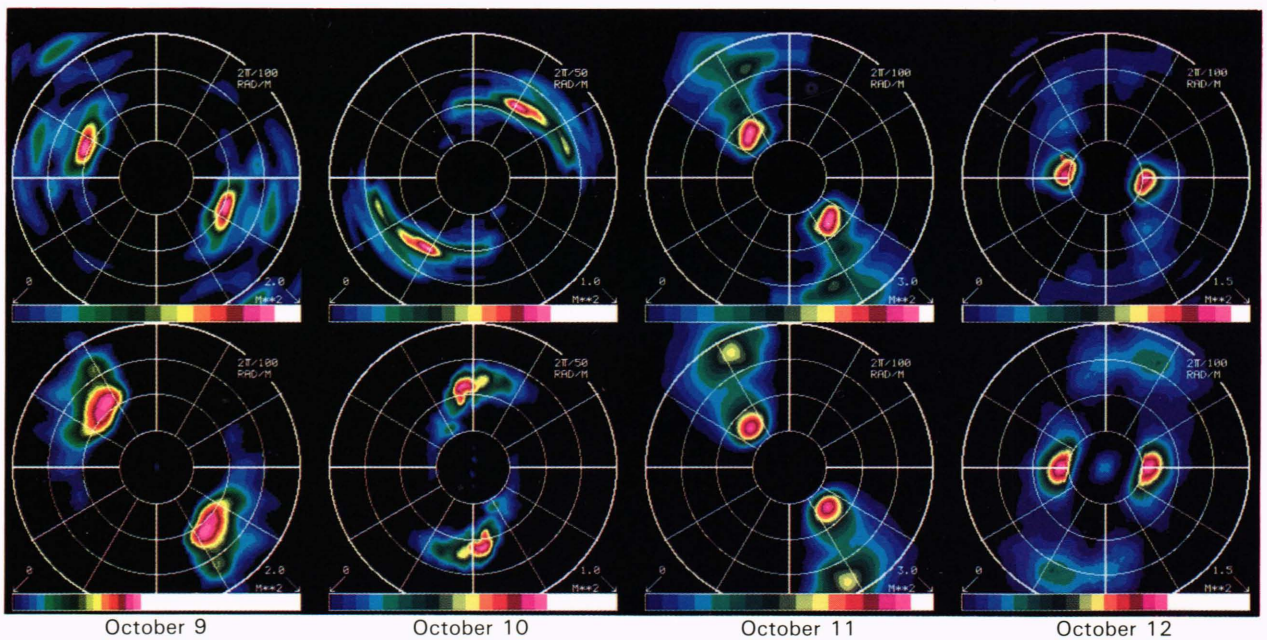

Figure 7—Estimates of wavenumber slope-variance spectra for the ROWS (top row) and SAR (bottom row) for each of the four days. The outer circle corresponds to 50 meters on the second day (October 10) only, and 100 meters on the remaining three days.

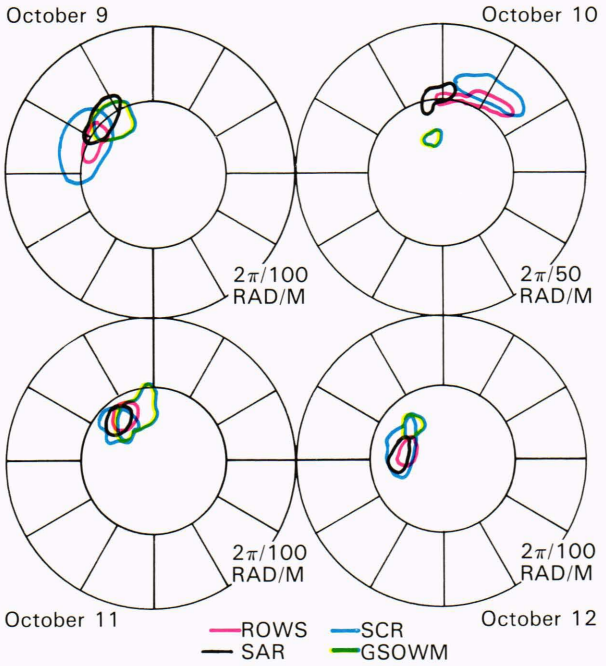

Figure 8—Estimates of half-power contours of the height-variance spectra from each of the four sources (SCR, ROWS, SAR, GSOWM) from October 9 (top left) through October 12 (bottom right).

for the lowest sea state, this failure can be totally ascribed to an error in angle about equal to the spectral width.

It should be emphasized that the apparent angular bias of GSOWM is not necessarily a result of a shortcoming in the model's physics, although this is certainly one possibility. After all, the model suffers severely from having practically no reliable inputs in the vast southern Pacific. In the absence of global wind-field estimates from a (future) satellite scatterometer, the ultimate cause for the discrepancy will remain speculative.

More important in this discussion are the apparent limitations of the SAR in faithfully reproducing the directional spectrum under all environmental conditions. Particularly noteworthy here is the indication that the SAR tends to perform better at high sea states than at low ones and that the lower bound of acceptable sea states lies in the region of 2- to 3-meters SWH. This hypothesis and its implications for an operational wave-monitoring concept will be pursued in the remainder of this article.

Implications for Global Monitoring of Waves

Using the dispersion relationship between frequency, ω, and wavenumber, k ($\omega^2 = gk$), an ocean wavelength, λ, is related to its period, T, by

$$\lambda = (g/2\pi)\, T^2 , \qquad (5)$$

and, from Eq. 4, the minimum detectable period, T_{min}, of an azimuth-traveling wave can be written

$$T_{min} = (4\pi/g)^{1/2} \left(\frac{R}{V}\right)^{1/2} H_s^{1/4} \cong 1.13 \left(\frac{R}{V}\right)^{1/2} H_s^{1/4} , \qquad (6)$$

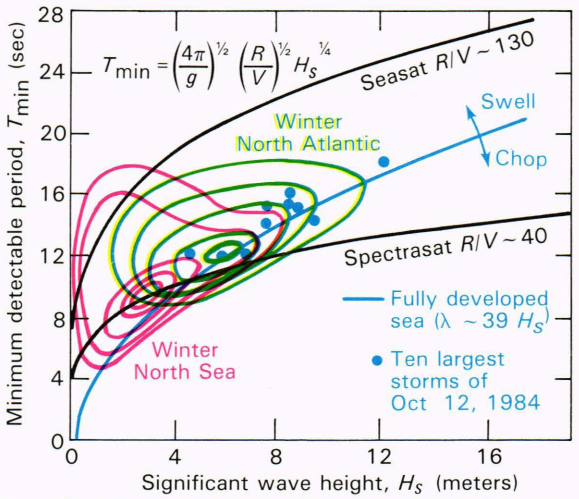

Figure 9—Joint probability densities, at the 0.1, 0.3, 0.5, 0.7, and 0.9 levels, of dominant period and SWH for both the winter North Atlantic and winter North Sea, superimposed on predicted SAR azimuth wavenumber limits for both a low (Spectrasat) and high (Seasat) altitude orbit. Also shown are the period-height relationships for a fully developed sea, and the corresponding U.S. Navy hindcasts for the ten largest storms of October 12, 1984.

with all units expressed in the meter-kilogram-second system. This relationship is plotted in Fig. 9 for two representative values of R/V, the higher R/V being 130, corresponding to Seasat (and approximately to the future European ERS-1), and the lower R/V being 40, corresponding to SIR-C (and approximately to Spectrasat, to be further described below). The two curves approximately define the lower bound of detectable azimuth-traveling waves as a function of their SWH. In general, short, high, growing seas are more difficult to properly image than long, low, decaying swells for the same range-to-velocity ratio.

Since the azimuth period limit increases only as $H_s^{1/4}$, whereas the dominant period of a fully developed sea increases as $H_s^{1/2}$ (i.e., the dominant wavelength, λ, is approximately 40 H_s), the more extreme storms are actually less likely to experience azimuth contamination than are the milder ones; this explains why SIR-B performed more poorly in the lower sea states. Major storm events are not necessarily well characterized by a fully developed spectrum, but the family of storms in Fig. 9 taken from GSOWM analyses for October 12, 1984, shows that the fully developed assumption is a reasonable approximation.

The fully developed relationship, when plotted on the other curves of Fig. 9, reveals the fundamental problem of attempting to image azimuth-traveling storm waves with large R/V platforms such as Seasat: even the largest storm on the planet failed to generate an azimuth wave of sufficiently long period to be detectable. On the other hand, for a lower altitude satellite at an R/V of 40, all fully developed seas of about 4 meters and higher generate sufficiently long azimuth waves to be detectable. This general conclusion appears slightly more restrictive than the specific examples from the SIR-B Chile data set discussed above, probably because the sea was not fully developed under SIR-B.

Typical Wave Climates

Since wave age (or steepness) clearly has a major impact on the probability of detection, the advantage of a low-altitude orbit can be further quantified with a more precise specification of the wave climate. For example, Fig. 9 contains two families of curves representing the joint period–height probability density for both the winter North Atlantic and the winter North Sea (from Ref. 7). The winter North Atlantic is characterized by (i.e., has a maximum joint probability of) 6-meter waves of 12-second period, while the winter North Sea is best characterized by 3-meter waves of 9-second period, although it also shows more than a normal amount of long low swell, presumably leaking in from the North Atlantic.

By integrating the joint probability densities as a function of R/V (which is nearly proportional to altitude for a low-orbiting spacecraft), an azimuth wave detection probability as a function of R/V can be extracted. Figure 10 shows the results of such an integration for the two regions and further illustrates the futility of attempting to image azimuth-traveling waves from high altitudes. Even at a low R/V, corresponding to an altitude of 275 kilometers, there is significant degradation, particularly in the North Sea. The probability of seeing azimuth-traveling waves from Seasat in the North Atlantic is practically zero. But from an altitude of 275 kilometers, about the lowest practical (see Kilgus and Frain, this issue), one could anticipate successful imaging of azimuth-traveling waves over 80 percent of the time.

SATELLITE SYSTEM IMPLICATIONS: SPECTRASAT

Advantage of a SAR/ROWS Combination

Although directional wave energy estimates appear to be practical from a spaceborne SAR in the open ocean, there are severe constraints on the orbit. To minimize azimuth filtering, the spacecraft must be placed at the lowest practical altitude. Even then, some filtering will be experienced, especially in steep seas and limited fetch bodies of water such as the North Sea.

The combination of a SAR and a ROWS on a common platform appears attractive for several reasons. The ROWS yields redundant absolute-energy estimates through a transfer function directly related to the wave-slope spectrum; its tranfer function appears well behaved and at most weakly dependent on the local environment; and it is one of the few techniques (aside from SAR) that is amenable to spacecraft implementation. Conversely, the ROWS has some weaknesses that can be overcome by SAR: it does not produce images, so cannot be used to monitor individual wave statistics and extreme wave probabilities (Mollo-Christensen, this issue; Tilley, this issue); it can suffer from cross-track smear, exactly complementary to the SAR along-track smear (Jackson, second of two articles, this issue); and it cannot follow the evolution of wave systems close to storm centers with the spatial resolution that is possible in SAR (Gonzalez et al., this issue).

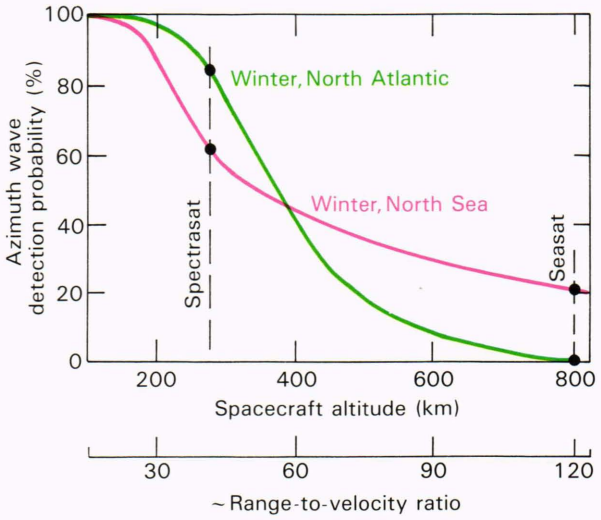

Figure 10—Estimated probability of detecting SAR azimuth-traveling waves as a function of spacecraft altitude and range-to-velocity ratio for two separate wave climates.

SAR/ROWS/Altimeter Footprint

Figure 11 shows the resulting Spectrasat[8] configuration obtained by combining a SAR, a ROWS, and a nadir-looking radar altimeter, along with their associated ground footprints. To maximize global sampling from a single satellite, two SAR antennas, each looking to an opposite side of nadir, are time shared from a common transmitter. With each SAR transmitter beam pointed 30 degrees from nadir, the swath separations are about equal to the spacecraft altitude. The rotation rate of the ROWS antenna is chosen to yield 3 revolutions every 250 kilometers of spacecraft travel (about 12 seconds per revolution), and the ROWS is activated for 1½ cycles out of each 3, for a 50 percent duty cycle. Each half cycle yields one complete independent directional spectrum over spatial scales of the order of 50 kilometers.

The SAR is activated for 100 kilometers out of every 250 kilometers, exactly complementary to the ROWS, and the SAR spectra are split evenly between two 50-kilometer samples on either side of nadir. The nadir-looking altimeter is activated simultaneously with the ROWS and also for a short sample between opposing SAR samples. The goal here is to interleave the various spectral estimates as much as possible within a 250-kilometer-square sampling area (which is also the spacing of GSOWM grid points at the equator) while minimizing the total power requirements of the spacecraft. In addition, the sampling is designed to permit various intercomparisons and cross-checks among the sensors on a quasicontinuous basis. Variations of the sampling are possible and may be desirable for some meteorological situations.

Output Data Rates

It is often assumed that a spaceborne SAR inherently creates such voluminous data rates as to overwhelm conventional SAR processing, transmission, and storage techniques. While this assumption may be valid for high-

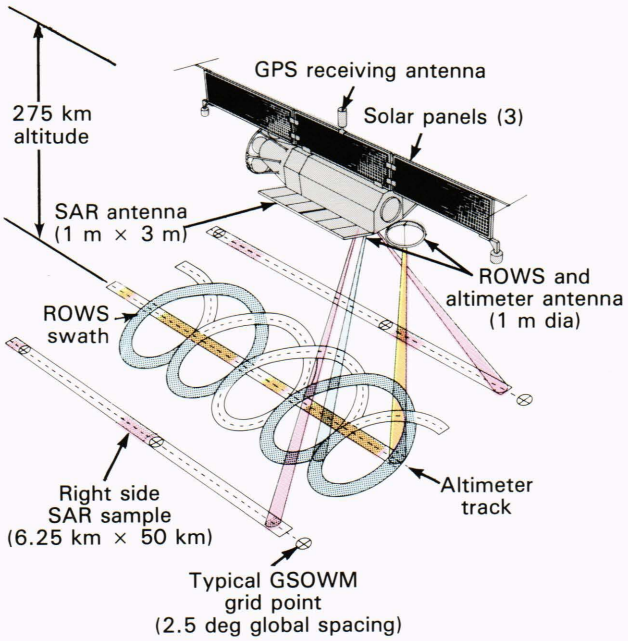

Figure 11—The low-altitude Spectrasat configuration, using a right- and left-looking SAR in conjunction with a ROWS and a nadir-looking altimeter.

resolution, large-swath imaging modes, the global collection of spectra presents a relatively small problem when the system parameters are well chosen. For example, consider a comparison between representative sets of system parameters, shown in Table 2, for both Seasat and Spectrasat.

By tailoring the satellite design to minimize both the number of cross-track samples (principally by narrowing the swath) and the azimuth compression ratio (resulting from transmitting C band at a lower altitude), it is possible to fit the spectral processing problem into a 256- × 256-square format. Such a format allows an on-board real-time processor design based on commercially available 1-megabit computer chips. By using postprocess spectral smoothing followed by along-track averaging of eight consecutive 6.4-kilometer-square spectral estimates, that is, by producing one high-confidence spectral estimate every 50 kilometers, the output data rate can easily be reduced to only a few kilobits per second. With identical spectral and spatial averaging, the ROWS data rate can match that of the SAR, and because they are time-shared, the resulting data rate, yielding one spectrum from either the SAR or ROWS every 50 kilometers, need not exceed a few kilobits per second. (MacArthur, this issue, gives more details on a practical system implementation.)

Table 2—Seasat versus Spectrasat processing constraints.

Cross Track	*Seasat*	*Spectrasat*	*Ratio*
Swath width	100 km	6.4 km	≈15
Sampling interval	12.5 m	25 m	2
Samples per swath	8000	256	≈30
Along Track			
Range	850 km (23°)	320 km (≤30°)	2.7
Wavelength	23 cm	5.5 cm	4.2
Sampling interval	6 m	8 m	
Synthetic aperture	8 km	550 m	
Azimuth compression	≈1300	≈65	≈20
Azimuth resolution	25 m (4 looks)	32 m (4 looks)	

SUMMARY

Although local wave climate can be a significant factor in assessing the probability of SAR azimuth contamination, it still appears that very-low-altitude orbits are necessary to reduce the contamination to an acceptable level. Even then, the short steep waves commonly found in limited fetch bodies of water will cause excess motion blur. For this reason and many others, the combination of a SAR and a ROWS on a common low-altitude satellite appears especially attractive. Each instrument, in effect, both verifies and complements the other. With a judicious choice of system parameters and geometry, on-board SAR processing to yield real-time spectra at a low data rate appears well within present technology. The combination of SAR and ROWS could yield continuous high-confidence spectral estimates at a rate of one spectrum every 50 kilometers of spacecraft travel, with an associated data rate well within 10 kilobits per second.

REFERENCES

[1] D. Atlas, R. C. Beal, R. A. Brown, P. DeMey, R. K. Moore, C. G. Rapley, and C. T. Swift, "Problems and Future Directions in Remote Sensing of the Ocean's Troposphere: A Workshop Report," *J. Geophys. Res.* **91**, 2525-2548 (1986).

[2] R. C. Beal, T. W. Gerling, D. E. Irvine, F. M. Monaldo, and D. G. Tilley, "Spatial Variations of Ocean Wave Directional Spectra from the Seasat Synthetic Aperture Radar," *J. Geophys. Res.* **91**, 2433-2449 (1986).

[3] R. C. Beal, F. M. Monaldo, D. G. Tilley, D. E. Irvine, E. J. Walsh, F. C. Jackson, D. W. Hancock III, D. E. Hines, R. N. Swift, F. I. Gonzalez, D. R. Lyzenga, and L. F. Zambresky, "A Comparison of SIR-B Directional Ocean Wave Spectra with Aircraft Scanning Radar Spectra and Global Spectral Ocean Wave Model Predictions," *Science* **232**, 1531-1535 (1986).

[4] F. C. Jackson and W. T. Walton, "Aircraft and Satellite Measurement of Ocean Wave Directional Spectra Using Scanning-Beam Microwave Radars," *J. Geophys. Res.* **90**, 987-1004 (1985).

[5] R. O. Harger, *Synthetic Aperture Radar Systems—Theory and Design*, Academic Press, New York, p. 36 (1970).

[6] F. M. Monaldo and D. R. Lyzenga, "On the Estimation of Wave Slope- and Height-Variance Spectra from SAR Imagery," *IEEE Trans. Geosci. Remote Sens.* **GE-24**, 543-551 (1986).

[7] *U. S. Navy Hindcast Spectral Ocean Wave Model Climatic Atlas: North Atlantic Ocean*, NAVAIR 50-1C-538, Naval Oceanography Command Detachment, Asheville, N.C., p. 118, sequence numbers 10 and 14 (Jan 1983).

[8] R. C. Beal, "Spectrasat: A Concept for the Collection of Global Directional Wave Spectra," in *Proc. International Geoscience and Remote Sensing Symposium*, Strasbourg, France, pp. 781-786 (1984).

ACKNOWLEDGMENTS—The spectral comparisons presented here required the cooperation of many members of the SIR-B Extreme Waves Team. E. Walsh, F. Jackson, and L. Zambresky provided formatted digital tapes from the SCR, ROWS, and GSOWM, respectively. SIR-B spectra were generated, corrected, and reformatted by F. Monaldo and D. Tilley from calibrated SAR image tapes provided by the Jet Propulsion Laboratory. T. Gerling computed temporal, spatial, and spectral interpolations from the GSOWM. Finally, D. Tilley color coded, normalized, and formatted the individual spectra for readout on an Optronics P-1700 film writer.

This work was supported by NASA Headquarters, the Office of Naval Research, and APL Independent Research and Development funds.